

Real-time Attacks Against Deep Reinforcement Learning Policies

Buse G. A. Tekgul
Aalto University

buse.atlitekgul@aalto.fi

Shelly Wang
University of Waterloo

shelly.wang@uwaterloo.ca

Samuel Marchal
F-Secure Corporation

samuel.marchal@aalto.fi

N. Asokan
University of Waterloo

asokan@acm.org

Abstract

Recent work has discovered that deep reinforcement learning (DRL) policies are vulnerable to adversarial examples. These attacks mislead the policy of DRL agents by perturbing the state of the environment observed by agents. They are feasible in principle but too slow to fool DRL policies in real time. We propose a new attack to fool DRL policies that is both effective and efficient enough to be mounted in real time. We utilize the Universal Adversarial Perturbation (UAP) method to compute effective perturbations independent of the individual inputs to which they are applied. Via an extensive evaluation using Atari 2600 games, we show that our technique is effective, as it fully degrades the performance of both deterministic and stochastic policies (up to 100%, even when the l_∞ bound on the perturbation is as small as 0.005). We also show that our attack is efficient, incurring an online computational cost of 0.027ms on average. It is faster compared to the response time (0.6ms on average) of agents with different DRL policies, and considerably faster than prior attacks (2.7ms on average). Furthermore, we demonstrate that known defenses are ineffective against universal perturbations. We propose an effective detection technique which can form the basis for robust defenses against attacks based on universal perturbations.

1. Introduction

Machine learning models are vulnerable to *adversarial examples*: maliciously crafted inputs generated by adding small perturbations to the original input in order to force a model into generating wrong predictions [24, 7]. Prior work [8, 11, 13, 26] has shown that adversarial examples can also fool deep reinforcement learning (DRL) agents using deep neural networks (DNNs) to approximate their *policy*: the decision-making strategy. If this vulnerability is ex-

ploited in safety-critical applications such as robotic surgery and autonomous driving, the impact can be disastrous.

A DRL agent can partially or fully observe the *state* of the environment by capturing complex, high-dimensional observations. For example, a DRL agent playing an Atari 2600 game observes pixels from each image frame of the game to construct states by combining a number of observations. DRL agents use the current state as an input to their policy which outputs a suitable action for that state. Consequently, adversaries can change the environment to mislead the agent’s sequential decision-making process. Various state-of-the-art attack methods assume *white-box* knowledge, where adversaries have access to the parameters of the agent’s policy model and the reinforcement learning algorithm. In *untargeted* attacks, instead of forcing the agent into performing specific actions, the adversary’s goal is to fool the agent’s policy so that the agent becomes useless. The agent is useless when it 1) cannot complete its task or 2) finishes its task with unacceptably poor performance. Prior work has shown that adversaries with white-box knowledge can successfully destroy an agent’s performance using one-step gradient-based approaches [7], optimization-based methods [5], or adversarial saliency maps [19]. Previous work has also proposed different attack strategies where the adversary generates the perturbation for 1) each state [8, 2], 2) *critical states* where the agent prefers one action with high confidence [13, 11, 22], or 3) periodically, at every N ’th state [11].

Although prior white-box attack strategies are effective in principle, they are not realistic in practice. First, some attack strategies [8, 13] are based on computing the perturbation using back-propagation or solving an optimization problem. This is computationally expensive even if it is done for every N ’th state. In DRL, agents’ response to a new state is quite fast – Attacks that take longer than the average time between two consecutive observations and the agent response time are too slow to be implemented in real-

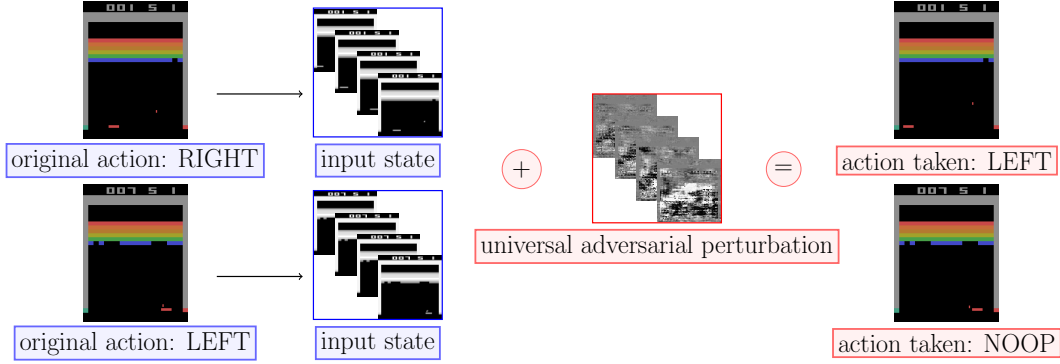


Figure 1: When added to the state, universal adversarial perturbation causes the victim policy to take another action than the original one. The victim agent fails to catch the ball and loses the game.

time. Secondly, in realistic scenarios, the adversary cannot have full control over the environment. In contrast, iterative attacks [13, 26] require querying agents with multiple perturbed versions of the current state and resetting the environment in order to find the optimal perturbation. Therefore, iterative attacks cannot be applied in real-life scenarios such as autonomous agents interacting with a dynamic environment. Finally, the aforementioned state-the-art attacks require collecting all observations of the current state before generating a perturbation. However, the agent can store clean observations that are part of the current state in its short-term memory before the current state is fully observed. In order to overcome these challenges, Xiao *et al.* [26] proposed a new attack strategy by producing a single, *universal perturbation* during the task. This method generates perturbations that are independent of the input state and can be mounted in real time. However, it needs to suspend the task (stopping the agent or the environment) for generating the perturbation and produce different perturbations for each episode *online*.

Contributions. We propose an effective, *real-time* attack strategy to fool DRL policies by computing universal perturbations (Figure 1) *offline*. Similar to previous work, we focus on untargeted attacks in a white-box setting. Our contributions are as follows:

1. We propose two novel real-time white-box attacks, UAP-S and UAP-O, that use Universal Adversarial Perturbation (UAP) [17] to generate state-agnostic adversarial examples against DRL policies (Section 3). An empirical evaluation of UAP-S and UAP-O using three different reinforcement learning algorithms playing three different Atari 2600 games demonstrates that both techniques are comparable to prior work in their effectiveness (100% drop in return) while being significantly faster (0.027 ms on average, compared to 2.7 ms) and less visible (Section 4.2).
2. We demonstrate that universal perturbations can evade

prior defenses [14, 27] that can detect and mitigate state-of-the-art attacks in DRL (Section 5.1).

3. We propose an efficient detection method, AD³, to detect the presence of different attacks. AD³ can be combined with other defenses to provide stronger resistance for DRL agents against adversarial examples. (Section 5.2).

2. Background

2.1. Deep reinforcement learning

Reinforcement Learning. In reinforcement learning, an agent and the environment interact with each other sequentially. At time step t , the environment is characterized by its state $s \in \mathcal{S}$ consisting of N past observations o pre-processed by some function f_{pre} , i.e., $s = \{f_{pre}(o_{t-N+1}), \dots, f_{pre}(o_t)\}$. At each s , the agent takes an action $a \in \mathcal{A}$ which moves the environment to the next s' and yields a reward r from the environment. The agent uses this information to optimize its policy π , a probability distribution that maps states into actions [23]. In the training phase, the agent iteratively updates the value function $V^\pi(s)$ or the action-value function $Q^\pi(s, a)$. $V^\pi(s)$ estimates how valuable it is to be in a state s by calculating the *expected discounted return*: the discounted cumulative sum of future rewards while following a specific π . Similarly, $Q^\pi(s, a)$ estimates the value of taking action a in the current state s . During evaluation, the optimized π is used for decision making, and the *performance* of the agent is measured by the return. We focus on *episodic* tasks, particularly Atari games, where each episode ends with a terminal state (e.g., winning/losing a game, arriving at a destination state). For each episode, the return is computed by the total score in single-player games (e.g., Breakout) or the difference between scores in competitive two-player games (e.g., Pong). **DNN.** DNNs are parameterized functions $f(x, \theta)$ that consists of neural network layers. For an input $x \in \mathbb{R}^n$ with n

input features, the parameter vector θ is optimized by training the DNN over a labeled training set. $f(\mathbf{x}, \theta)$ outputs a vector $\mathbf{y} \in \mathbb{R}^m$. In classification problems, one can find the predicted class as $\hat{f}(\mathbf{x}) = \operatorname{argmax}_m f_m(\mathbf{x}, \theta)$, where f_m corresponds to output of $f(\mathbf{x}, \theta)$ for class m . For simplicity, we will use $f(\mathbf{x})$ to denote $f(\mathbf{x}, \theta)$.

DRL. Since DNNs are natural function approximators, they are useful for approximating π when \mathcal{S} or \mathcal{A} is too large, or largely unexplored. Deep Q Networks (DQN) is one of the well-known *value-based* DRL algorithm [16] that uses DNNs to approximate $Q^\pi(s, a)$. DQN first obtains the optimal action-value function $Q^*(s, a)$ by solving $\max_\pi (Q^\pi(s, a))$, then infers the optimal π implicitly using $Q^*(s, a)$. *Policy-based* methods employ DNNs to directly parameterize π with a parameter vector θ . These methods update θ by applying gradient descent algorithms. Finally, in *actor-critic* methods, the critic function estimates $Q^\pi(s, a)$ or $V^\pi(s)$ for the current π and the actor function updates θ of π using the direction provided by the critic.

2.2. Adversarial examples

An adversarial example \mathbf{x}^* against a classification model $f(\mathbf{x})$ is a deliberately modified version of an input \mathbf{x} such that \mathbf{x} and \mathbf{x}^* are similar, but \mathbf{x}^* is misclassified by f , i.e., $\hat{f}(\mathbf{x}) \neq \hat{f}(\mathbf{x}^*)$. An untargeted adversarial example is found by solving

$$\begin{aligned} & \operatorname{argmax}_{\mathbf{x}^*} \ell(f(\mathbf{x}^*), \hat{f}(\mathbf{x})) \\ & \text{s.t.: } \|\mathbf{x}^* - \mathbf{x}\|_p = \|\mathbf{r}\|_p \leq \epsilon, \end{aligned} \quad (1)$$

where ϵ is the l_p perturbation constraint and ℓ is the loss between $f(\mathbf{x}^*)$ and the predicted label $\hat{f}(\mathbf{x})$. In this work, we assume the l_∞ constraint (i.e., any element in the perturbation must not exceed than a specified threshold ϵ) as in the state-of-the-art Fast Gradient Sign Method (FGSM) [7]. FGSM calculates an adversarial perturbation \mathbf{r} by

$$\mathbf{r} = \epsilon \cdot \operatorname{sign}(\nabla_{\mathbf{x}} \ell(f(\mathbf{x}), \hat{f}(\mathbf{x}))). \quad (2)$$

Usually, adversarial examples are generated specifically for each \mathbf{x} . An alternative is to generate input-agnostic *universal perturbations*. For instance, *Universal Adversarial Perturbation* (UAP) [17] searches for a sufficiently small \mathbf{r} that can be added to *arbitrary* inputs to yield adversarial examples against f . In UAP, the adversary iteratively computes \mathbf{r} that fools the classifier for almost all inputs \mathbf{x} belonging to a training set \mathcal{D}_{train} . In addition to the l_∞ constraint, perturbations should achieve a desired *fooling rate* δ : the proportion of successful adversarial examples against f with respect to the total number perturbed samples $|\mathcal{D}|$ in a dataset \mathcal{D} .

2.3. Adversarial examples against DRL policies

To find an adversarial example against a DRL policy, Equation 1 is modified by changing the input \mathbf{x} into s at

time t , and replacing f with π . Given s and $\pi(s)$, $\hat{\pi}(s)$ outputs the most suitable action. We also denote $\pi_m(s)$ as the log probability of m -th action for s . In this setup, adversarial examples are computed to mislead either Q or π . For simplicity, we will use $\pi(s)$ to denote Q in value-based methods and π in policy-based methods.

Prior work implemented well-known adversarial example generation methods such as FGSM [8, 11], JSMA [2] and Carlini&Wagner [13] against DRL policies. These methods effectively decrease the return of the agent, but they cannot be implemented in real-time and have a temporal dependency: they need to compute a different \mathbf{r} for every s . Xiao *et al.* [26] propose a type of universal perturbation “obs-seq-fgsm-wb”: applying FGSM to averaged gradients over k states to compute \mathbf{r} and adding it to the remaining states in that episode. However, it still needs to compute \mathbf{r} for every new episode, and interferes with the task during the generation of \mathbf{r} .

2.4. Defending against DRL adversarial examples

Prior work [11, 3] demonstrate that adversarial training improves the resilience to adversarial perturbations and recovers the performance of v . However, Zhang *et al.* [27] prove that adversarial training leads to a performance degradation and is not robust against strong attacks. In order to overcome the challenges of adversarial training, Zhang *et al.* [27] propose state-adversarial Markov decision process (SA-MDP). SA-MDP aims to find an optimal π under the strongest adversary using policy regularization. This regularization technique helps DRL agents maintain their performance even against adversarially perturbed inputs.

Another defense method is Visual Foresight [14]: a module trained to predict the current observation \hat{o}_t at time t using k previous observations $o_{t-k} : o_{t-1}$ and corresponding actions $a_{t-k} : a_{t-1}$. Visual foresight also predicts the possible action \hat{a}_t for the partially predicted \hat{s} using π , where $\hat{s} = \{f_{pre}(o_{t-N+1}), \dots, f_{pre}(\hat{o}_t)\}$. The difference between $\pi(\hat{s})$ and $\pi(s)$ is used to detect the presence of adversaries, and \hat{a}_t is selected to retain the performance of v .

3. State and observation agnostic attacks

We first define our adversary model and then formally present two new attacks, which we call state-agnostic UAP (UAP-S) and observation-agnostic UAP (UAP-O).

3.1. Adversary model

Adversary’s goal. The goal of the adversary Adv is to degrade the performance of the victim DRL agent v by adding perturbations \mathbf{r} to s . Adv is successful when the attack:

1. is *effective*, i.e., limits v to a low return,
2. is *efficient*, i.e., can be realized in real-time, and

3. *evades* known defenses.

Adversary’s capabilities. *Adv* has a complete knowledge of π_v and the DRL algorithm. *Adv* is also capable of perturbing s by physically altering the environment (e.g., inserting a physical object into the environment, changing road conditions in autonomous driving, or changing pixel values of a video stream). However, *Adv* is constrained to only using r with a small norm to evade possible detection, either by specific anomaly detection mechanisms or via human observation. In addition, we assume that *Adv* cannot reset the environment or return to an earlier state. In other words, we deem that other arbitrary attacks (e.g., swapping one frame with another or changing observations with random noise) can be easily detected.

3.2. Attack design

To generate UAP-S and UAP-O, *Adv* first collects a training set \mathcal{D}_{train} by monitoring the environment for one episode and saving each s into \mathcal{D}_{train} . Simultaneously, *Adv* copies the weights of v ’s policy network π_v into a proxy policy π_{adv} . Therefore, *Adv* can obtain r without interrupting v or the environment. *Adv* sanitizes \mathcal{D}_{train} by choosing only the *critical states*. Following [13], we define critical states as those that can have a significant influence on the course of the episode. We identify critical states by using the relative action preference function defined as:

$$\text{Var}(\text{Softmax}(\pi_{adv}(s))) \geq \beta, \quad (3)$$

modified from [13], where Var is the variance of Softmax values computed for each action m . We calculate β by averaging $\text{Var}(\text{Softmax}(\pi_{adv}(s)))$ over all $s \in \mathcal{D}_{train}$. This ensures that both UAP-S and UAP-O fool π mostly in critical states and remain undetected in trivial states.

For both UAP-S and UAP-O, we assume that $s \in \mathcal{D}_{train}$ and $\mathcal{D}_{train} \subset \mathcal{S}$. *Adv* searches for an optimal r that satisfies the constraints presented in Section 2.2. For generating UAP-S, we implement the original method in [17] (see Section 2.2) that uses the DeepFool algorithm to solve Equation 1. In UAP-S, there is a different perturbation for each observation o_j in s , i.e., $r = \{r_{t-N+1}, \dots, r_t\}$, $r_j \neq r_k, \forall j, k \in \{t-N+1, \dots, t\}, j \neq k$. In contrast, for UAP-O, the same perturbation is applied to all observations in s . Therefore, it can be considered as a completely universal attack. UAP-O aims to find a modified version \tilde{r} of r by solving

$$\min(\|r - \tilde{r}\|_2^2) \quad (4)$$

$$\text{s.t.}: \tilde{r}_j = \tilde{r}_k, \quad \forall j, k \in \{t-N+1, \dots, t\} \text{ and } \|\tilde{r}\|_\infty \leq \epsilon.$$

Equation 4 can be solved by adding an additional step to the DeepFool algorithm. DeepFool computes r iteratively and updates the perturbed s_i^* until π outputs a wrong action

(see Algorithm 2 in [18]). At each iteration i , DeepFool finds the closest hyperplane $\hat{l}(s_i^*)$ and r_i that projects s_i^* on the hyperplane. It re-computes r_i as

$$\begin{aligned} \pi'_i &\leftarrow \pi_{adv_i}(s_i^*) - \pi_{adv_{m_s}}(s_i^*), \\ w'_i &\leftarrow \nabla \pi_{adv_i}(s_i^*) - \nabla \pi_{adv_{m_s}}(s_i^*), \\ r_i &\leftarrow \frac{|\pi'_i|}{\|w'_i\|_2^2} w'_i, \end{aligned} \quad (5)$$

where ∇ is the gradient of π_{adv} w.r.t s_i and $\pi_{adv_{m_s}}$ is the log likelihood of the m -th action that was chosen for the clean state s . The closest \tilde{r}_i to r_i satisfying the conditions in Equation 4 is found by averaging w'_i over the time dimension:

$$\tilde{r}_{i_j} = 1/N \sum_{k=(t-N+1)}^t w'_{i_k}, \quad \forall j \in \{t-N+1, \dots, t\}. \quad (6)$$

The DeepFool algorithm returns $\tilde{r}_j = \sum_i \tilde{r}_{i_j}$ as the optimal perturbation. UAP-O adds the same perturbation \tilde{r}_j to every observation o_j in s . The proof for Equation 6 can be found in Appendix A.

4. Attack evaluation

We evaluated the effectiveness of UAP-S and UAP-O on three Atari 2600 games (Pong, Breakout, Freeway) in the Arcade Learning Environment [4].

4.1. Experimental setup

To provide an extensive evaluation, for every game, we trained three agents each using a different DRL algorithm: value-based DQN [16], policy-based PPO [21] and actor-critic method A2C [15]. We used the same DNN architecture as in [16] for approximating Q in DQN and π for other algorithms. Our implementations of DQN, PPO and A2C are based on OpenAI baselines [6], and our victim agents achieve similar returns as in OpenAI Baselines. For pre-processing, we converted each RGB observation to gray-scale, re-sized those from 210×160 to 84×84 , and normalized the pixel range from $[0, 255]$ to $[0, 1]$. We used the frame-skipping technique [16], where v constructs s at every N -th observation, then selects an action and repeats it until the next state s' . We set $N = 4$ so the input state size is $4 \times 84 \times 84$. We also kept the frame rate of each game as 60 Hz; thus, the time interval between consecutive states is $4/60 = 0.067$ seconds.

We implemented UAP-S and UAP-O by setting the desired δ on \mathcal{D}_{train} to 95%, so that both methods stop searching for another r when $\delta \geq 95\%$ on the perturbed \mathcal{D}_{train} . As baselines for comparison, we started with FGSM [8],

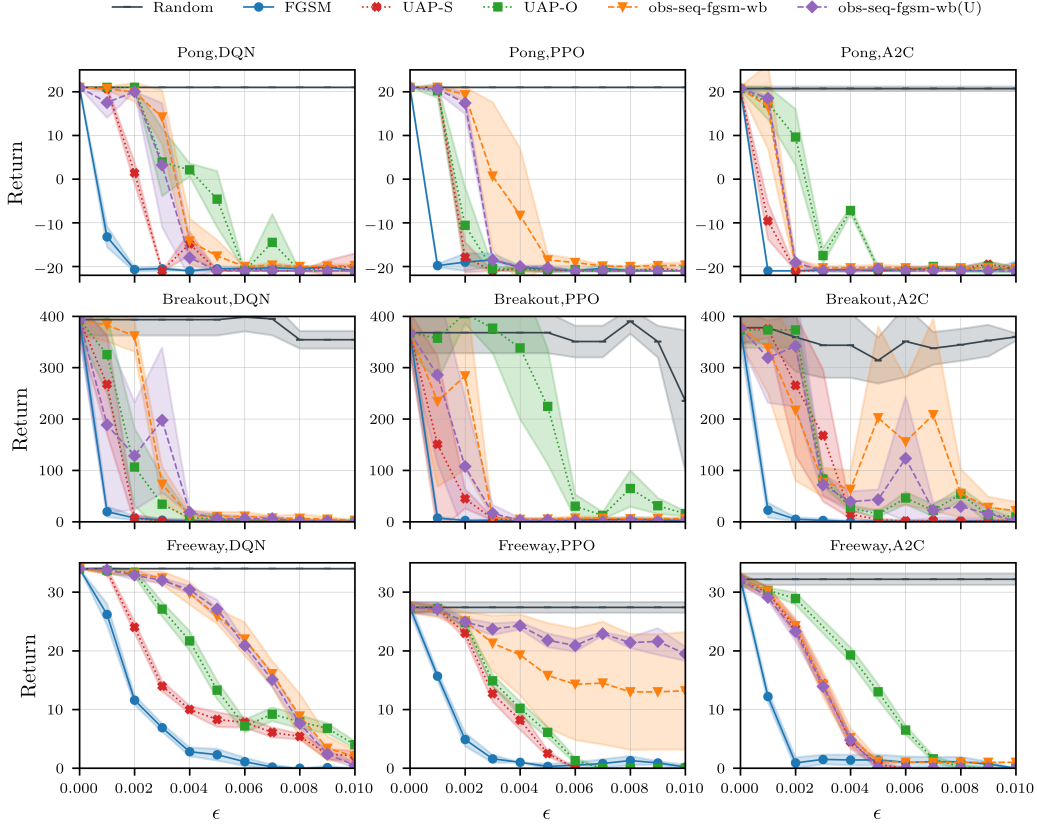


Figure 2: Comparison of attacks against three different policy networks (DQN, PPO, A2C) trained for three Atari games (Pong, Breakout, Freeway). The graph shows how the return (averaged over 10 games) changes with different ϵ values for six different attack strategies.

random noise addition and obs-seq-fgsm-wb [26]. We also used a variant of obs-seq-fgsm-wb so that the same \mathbf{r} is computed offline using the proxy policy π_{adv} during one episode, and applied to all other episodes. This variant generates a universal perturbation \mathbf{r} offline and mounts the attack in real-time. We call this variant obs-seq-fgsm-w(U) to indicate that it is a universal perturbation.

We measured the attack effectiveness where ϵ is between 0 and 0.01. We also reported the average return over 10 episodes and run each episode with a different seed during training and evaluation. To aid reproducibility, we summarized the required software packages in Appendix B.

4.2. Attack performance

Performance degradation. Figure 2 compares UAP-S and UAP-O with the four baseline attacks. As can be seen from the figure, random noise addition cannot cause a significant drop in v 's performance, while FGSM is the most effective attack reducing the return up to 100% even with a very small ϵ . UAP-S is the second most effective attack in almost every setup. UAP-S decreases the return by more than 50% in all

experiments when $\epsilon \geq 0.004$. The effectiveness of UAP-O, obs-seq-fgsm-wb, and obs-seq-fgsm(U) are comparable in different setups. We also observe that the effectiveness of obs-seq-fgsm-wb fluctuates heavily (A2C agent playing Breakout) or has high variance (PPO agent playing Freeway). This phenomenon is the result of obs-seq-fgsm-wb's inability to collect enough knowledge in order to generalize \mathbf{r} to the rest of the episode.

Timing comparison Table 1 presents the computational cost for generating \mathbf{r} (at $\epsilon = 0.01$) and the agent's response time (the time spent for feeding \mathbf{s} forward through π_v). Table 1 confirms that the online cost of obs-seq-fgsm-wb and FGSM is higher than all other attacks and, more importantly, v 's response time and the time interval between consecutive states. Thus, these attacks cannot be applied in real-time. UAP-S and UAP-O have a higher offline cost than obs-seq-fgsm-wb(U), but the offline generation of \mathbf{r} does not interfere with the task, since UAP-S and UAP-O do not require interrupting or pausing v . The online cost of UAP-S, UAP-O and obs-seq-fgsm-wb(U) is lower than v 's response time and the time interval between consecu-

Experiment	Attack method	Offline cost \pm std (seconds)	Online cost \pm std (seconds)
Pong, DQN, Agent's response time: $4 \times 10^{-4} \pm 10^{-6}$ sec	FGSM	-	$13 \times 10^{-4} \pm 10^{-5}$
	UAP-S	36.4 ± 21.1	$2.7 \times 10^{-5} \pm 10^{-6}$
	UAP-O	138.3 ± 25.1	$2.7 \times 10^{-5} \pm 10^{-6}$
	obs-seq-fgsm-wb	-	5.3 ± 0.1
	obs-seq-fgsm-wb(U)	5.3 ± 0.1	$2.7 \times 10^{-5} (\pm 10^{-6})$
Pong, PPO, Agent's response time: $9.3 \times 10^{-4} \pm 10^{-5}$ sec	FGSM	-	$21 \times 10^{-4} \pm 10^{-5}$
	UAP-S	41.9 ± 16.7	$2.7 \times 10^{-5} \pm 10^{-6}$
	UAP-O	138.3 ± 25.1	$2.7 \times 10^{-5} \pm 10^{-6}$
	obs-seq-fgsm-wb	-	7.02 ± 0.6
	obs-seq-fgsm-wb(U)	7.02 ± 0.6	$2.7 \times 10^{-5} \pm 10^{-6}$
Pong, A2C, Agent's response time: $9.3 \times 10^{-4} \pm 10^{-5}$ sec	FGSM	-	$21 \times 10^{-4} \pm 10^{-5}$
	UAP-S	11.4 ± 4.3	$2.7 \times 10^{-5} \pm 10^{-6}$
	UAP-O	55.5 ± 29.3	$2.7 \times 10^{-5} \pm 10^{-6}$
	obs-seq-fgsm-wb	-	7.2 ± 1.1
	obs-seq-fgsm-wb(U)	7.2 ± 1.1	$2.7 \times 10^{-5} \pm 10^{-6}$

Table 1: Offline and online comparison of attacks in terms of the time spent for the perturbation generation and mounting the attack in the test phase. Victim agents are DQN, PPO, A2C agents trained for Pong and $\epsilon = 0.01$. Attacks that cannot be implemented in real-time are in bold.

Attack Method	Real-time	Temporal dependency	Observation dependency
FGSM [8]	No	Dependent	Dependent
<u>UAP-S</u>	Yes	Independent	Dependent
<u>UAP-O</u>	Yes	Independent	Independent
obs-seq-fgsm-wb [26]	No	Dependent	Dependent
obs-seq-fgsm-wb(U) [26]	Yes	Independent	Dependent

Table 2: Summary of five attacks based on the characteristics that makes an attack plausible in a real deployment scenario. New attacks proposed in this paper are highlighted in blue and underlined.

tive states; therefore, they can be mounted in real-time.

Distortion difference. We compared the maximum amount of perturbation added into observations for different attacks. Figure 3 shows that perturbations obtained via UAP-S (and UAP-O in some cases) are smaller and less visible than other attacks for a given ϵ value, since UAP tries to find a minimal perturbation that sends all $x \in \mathcal{D}_{train}$ outside the decision boundary [17]. Therefore, UAP-S and UAP-O are less detectable, but they are efficient in decreasing v 's performance.

Table 2 summarizes the characteristics of all attacks implemented in the paper. As shown in the table, FGSM and obs-seq-fgsm-wb cannot be mounted in real-time and need pre-computation for each s or once in every episode. UAP-S, UAP-O and obs-seq-fgsm-wb(U) are real-time attacks that do not require stopping the agent or the environment while adding the perturbation. UAP-S and obs-seq-fgsm-wb(U) generate a perturbation that is independent from s , but the perturbation for each observation inside s are different. On the other hand, UAP-O can be considered as both observation- and state-agnostic: it adds the

same perturbation to all observations at any s , and can be mounted in real-time. In summary, despite its effectiveness, FGSM re-computes r for every s , which is infeasible. Both FGSM and obs-seq-fgsm-wb cannot be mounted in real-time. UAP-O leads to an efficient and effective attack when $\epsilon \geq 0.006$ even though it is the only attack with a unique perturbation that can be added into any o_j . UAP-S is the best attack considering both effectiveness and efficiency.

In simple environments like Atari 2600 games, sequential states are not i.i.d. Additionally, Atari 2600 games are *controlled* environments, where future states are predictable, and gameplays (i.e. episodes) do not deviate from one another for the same π_v . obs-seq-fgsm-wb and obs-seq-fgsm-wb(U) leverage this non-i.i.d property. However, their effectiveness might decrease in uncontrolled environments and the physical world due to the uncertainty of the future states. In contrast, UAP-S is independent of the correlation between sequential states. To confirm our conjecture, we implemented obs-seq-fgsm-wb(U) against VGG-16 image classifiers [28] pretrained on ImageNet [20], where ImageNet can be viewed as a non i.i.d., uncontrolled environment. We measured that obs-seq-fgsm-wb(U) achieves a fooling rate of up to 30% on the ImageNet validation set with $\epsilon = 10$, while UAP has a fooling rate of 78% [17], where the l_∞ norm of an image in the validation set is around 250. Therefore, we conclude that UAP-S can mislead π_v more than obs-seq-fgsm-wb(U) in complex, uncontrolled environments.

5. Detecting and mitigating universal attacks

A good defense for DRL agents against adversarial examples must be *resilient* enough to retain the agent's performance, and impose only minimal overhead (compared to the agent's response time) to be able to operate in real-time. While the detection of adversarial examples is useful, it is not sufficient by itself in safety-critical applications since in the absence of a resilient defense, v can only stop the task when an attack is detected.

5.1. Effectiveness of existing defenses

Although adversarial training [11, 3] presented promising results at defending against adversarial examples, it also leads to unstable training, performance degradation and is ineffective against strong attacks [27]. Moreover, Moosavi *et al.* [17] proved that despite a slight decrease in the fooling rate δ on the test set, Adv can easily compute another universal perturbation against retrained agents. Thus, directly applying adversarial retraining is not an effective defense against attacks using universal perturbations.

In order to show that universal perturbations can evade existing defenses, we implemented two methods that aim to retain the average return under attack: Visual Foresight [14] and SA-MDP [27] (Section 2.4). While we implemented

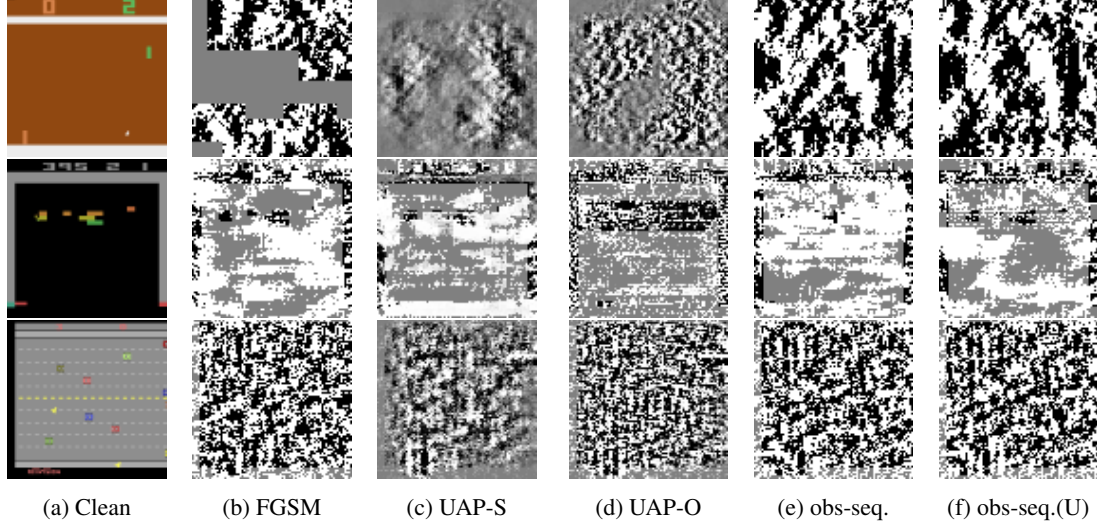


Figure 3: Comparison of the amount of perturbation added into the same clean observation in different attacks when $\epsilon = 0.01$. UAP-S and UAP-O generate smaller perturbations. Top row: DQN agent playing Pong, Middle row: PPO agent playing Breakout, Bottom row: A2C agent playing Freeway. In perturbation images, black pixels: -0.01 , white pixels: $+0.01$, gray pixels: 0.0 .

ϵ	Method	No attack	FGSM	Average Reward \pm std (Pong DQN / Freeway DQN)		obs-seq-fgsm-wb	obs-seq-fgsm-wb(U)
				UAP-S	UAP-O		
0.005	vanilla 1	21.0 \pm 0.0 / 34.0 \pm 0.0	-19.9 \pm 1.3 / 2.3 \pm 1.0	-21.0 \pm 0.0 / 8.3 \pm 1.3	-4.6 \pm 6.4 / 13.3 \pm 1.5	-17.6 \pm 3.6 / 25.9 \pm 1.3	-21.0 \pm 0.0 / 27.1 \pm 1.6
	Visual Foresight [14]	6.6 \pm 10.3 / 29.3 \pm 1.5	-20.5 \pm 0.5 / 29.6 \pm 1.8	-18.2 \pm 0.9 / 21.2 \pm 1.1	-14.6 \pm 2.5 / 21.9 \pm 1.3	-17.7 \pm 3.0 / 28.4 \pm 1.7	-21.0 \pm 0.0 / 27.7 \pm 1.0
	vanilla 2 [27]	21.0 \pm 0.0 / 33.9 \pm 0.3	-20.4 \pm 0.0 / 5.8 \pm 1.2	-/-	20.2 \pm 0.8 / 0.0 \pm 0.0	20.1 \pm 2.1 / 1.0 \pm 0.0	20.6 \pm 0.6 / 0.0 \pm 0.0
	SA-MDP [27]	21.0 \pm 0.0 / 30.0 \pm 0.0	21.0 \pm 0.0 / 30.0 \pm 0.0	-/-	21.0 \pm 0.0 / 30.0 \pm 0.0	21.0 \pm 0.0 / 30.0 \pm 0.0	21.0 \pm 0.0 / 30.0 \pm 0.0
0.01	vanilla 1	21.0 \pm 0.0 / 34.0 \pm 0.0	-20.9 \pm 0.3 / 0.0 \pm 0.0	-20.0 \pm 3.0 / 2.1 \pm 0.8	-21.0 \pm 0.0 / 4.0 \pm 0.6	-19.8 \pm 0.4 / 2.0 \pm 1.1	-21.0 \pm 0.0 / 0.5 \pm 0.5
	Visual Foresight [14]	6.6 \pm 10.3 / 29.3 \pm 1.5	-16.8 \pm 1.7 / 28.6 \pm 1.1	-20.5 \pm 0.5 / 22.8 \pm 0.4	-15.7 \pm 2.2 / 23.5 \pm 1.2	-11.9 \pm 7.5 / 26.6 \pm 1.6	-21.0 \pm 0.0 / 25.5 \pm 1.3
	vanilla 2 [27]	21.0 \pm 0.0 / 33.9 \pm 0.3	-20.7 \pm 0.4 / 2.3 \pm 0.9	-/-	0.2 \pm 12.5 / 0.0 \pm 0.0	-12.8 \pm 8.9 / 1.0 \pm 0.0	-12.3 \pm 9.6 / 0.0 \pm 0.0
	SA-MDP [27]	21.0 \pm 0.0 / 30.0 \pm 0.0	21.0 \pm 0.0 / 30.0 \pm 0.0	-/-	21.0 \pm 0.0 / 30.0 \pm 0.0	21.0 \pm 0.0 / 30.0 \pm 0.0	21.0 \pm 0.0 / 30.0 \pm 0.0
0.02	vanilla 1	21.0 \pm 0.0 / 34.0 \pm 0.0	-19.9 \pm 1.3 / 0.0 \pm 0.0	-21.0 \pm 0.0 / 0.1 \pm 0.3	-20.8 \pm 0.6 / 0.8 \pm 0.6	-20.0 \pm 0.0 / 1.0 \pm 0.0	-21.0 \pm 0.0 / 0.0 \pm 0.0
	Visual Foresight [14]	6.6 \pm 10.3 / 29.3 \pm 1.5	-14.5 \pm 3.5 / 27.2 \pm 1.9	-18.2 \pm 1.6 / 22.1 \pm 1.5	-15.5 \pm 1.8 / 24.4 \pm 0.7	-12.1 \pm 9.9 / 28.8 \pm 1.2	-20.8 \pm 0.4 / 29.3 \pm 1.7
	vanilla 2 [27]	21.0 \pm 0.0 / 33.9 \pm 0.3	-21.0 \pm 0.0 / 0.0 \pm 0.0	-/-	5.5 \pm -16.3 / 0.0 \pm 0.0	-20.5 \pm 0.5 / 1.0 \pm 0.0	-21.0 \pm 0.0 / 0.0 \pm 0.0
	SA-MDP [27]	21.0 \pm 0.0 / 30.0 \pm 0.0	-14.0 \pm 9.0 / 29.8 \pm 0.6	-/-	-21.0 \pm 0.0 / 29.4 \pm 1.2	-20.0 \pm 0.0 / 30.0 \pm 0.0	-21.0 \pm 0.0 / 30.0 \pm 0.0

Table 3: Average rewards over 10 episodes on DQN agents playing Pong and Freeway with or without any additional defense. Vanilla 1 models were generated by our implementation, while we downloaded vanilla 2 and SA-MDP models trained by convex relaxation from the repository https://github.com/chenhongge/SA_DQN provided by the authors. In each row, the best attack (lowest reward) is in bold font. The grey rows refer the least robust (lowest reward) defense methods for each attack.

Visual Foresight from scratch for our DQN models following the original experimental setup in [14], we downloaded other victim and SA-MDP models (trained by convex relaxation) for DQN agents from their reference implementation¹. These models only use one observation per s ; therefore, UAP-S would reduce to UAP-O for those models. Table 3 shows the average return under all attacks for agents with and without defenses (“vanilla”). Results show that Visual Foresight cannot maintain the performance of the DQN agent playing Pong. Moreover, it deteriorates the performance of the agent when there is no attack, and is less robust to universal attacks than FGSM and obs-seq-fgsm-wb. SA-MDP is a better defense than Visual Foresight but it still

¹https://github.com/chenhongge/SA_DQN

fails to defend any attack against the DQN agent playing Pong when $\epsilon \geq 0.02$. Therefore, in addition to a recovery technique, there should be an additional mechanism to detect when the agent is under attack. In Section 5.2 we propose such a detection mechanism that can be combined with existing recovery mechanisms.

5.2. Action Distribution Divergence Detector (AD³)

In a typical DRL episode, the sequential actions exhibit some degree of *temporal coherence*: the likelihood of the agent selecting a specific current action given a specific last action is consistent across different episodes. We also observed the temporal coherence is disrupted when the

Game	Parameter Values	Precision / Recall
Pong	$k_1 = 12, k_2 = 24,$	1.0/ 1.0 for all ϵ except for obs-seq-fgsm-wb at $\epsilon = 0.005$
	$t_1 = 400, t_2 = 200,$ $p = 400, r = 100.$	
Freeway	$k_1 = 12, k_2 = 24,$	1.0/ 1.0 for all ϵ
	$t_1 = 400, t_2 = 200,$ $p = 400, r = 90.$	

Table 4: Optimal values of AD³ to detect attacks with parameters specified in Table 3.

episode is subjected to an attack. We leverage this knowledge to propose a detection method, Action Distribution Divergence Detector (AD³), that calculates the statistical distance between the *conditional action probability distribution* (CAPD) of the current episode to the learned CAPD in order to detect whether the agent is under attack.

To train AD³, v first runs k_1 episodes in a safe and controlled environment before the deployment. AD³ records all actions taken during that time and approximates the conditional probability of the next action given the current one using the bi-gram model. We call the conditional probability of actions approximated by k_1 episodes as the *learned* CAPD. Second, to differentiate between the CAPD of a normal game versus a game that is under attack with high confidence, v runs another k_2 episodes in a safe environment. AD³ decides a threshold value th where the statistical distance between the CAPD of the normal game and the learned CAPD falls mostly under this threshold. We use Kullback–Leibler (KL) divergence [12] as the statistical distance measure. KL divergence between the learned CAPD and the CAPD of the current episode is calculated at each time-step starting after the first t_1 steps. We skipped the first t_1 time-steps because the CAPD of the current episode is initially unstable and KL divergence is naturally high at the beginning of every episode. We set the threshold th as the p^{th} percentile of all KL-divergence values calculated for k_2 episodes. During deployment, AD³ continuously updates the CAPD of the current episode, and after t_1 time-steps, calculates the KL-divergence between the CAPD of the current episode and the learned CAPD. If the KL-divergence exceeds the threshold th by $r\%$ or more during a time window t_2 , then AD³ raises an alarm that the agent is under attack.

We perform a grid search to find optimal values for the parameters used in this detection module and choose the parameters with the best F1-score. Optimal parameter values found from the grid search can be found in Table 4 for attacks with the same parameters as in Table 3. Using these optimal parameters, AD³ detects all five attacks with different ϵ bounds with nearly perfect recall and precision with the exception of obs-seq-fgsm-wb at $\epsilon = 0.005$ in Pong that has a precision of 1.0 and recall of 0.8. AD³ can be com-

bined with Visual Foresight, SA-MDP or other defenses to improve the defense against adversarial examples.

6. Related Work

Targeted white-box attacks. In targeted attacks, Adv ’s goal is to lure v into a specific s or to force v into following a specific path defined by Adv . Enchanting attack [13] is a targeted attack that steers π_v into a targeted s . This attack uses an iterative method [5] to craft perturbations for a series of states, which is too slow in real-time. Another targeted attack [25] uses the Adversarial Transformer Network [1] to misguide π_v into optimizing a reward function defined by Adv . Although this attack is faster than FGSM, it still requires observing the full s before generating the perturbation. The CopyCat attack [9] is a targeted attack that uses pre-computed perturbations. It generates different perturbations for each action to force π_v into following Adv ’s policy π_{adv} . This attack only applies perturbations to the last o inside s . Both attack methods in [25, 9] can be easily detected and mitigated by Visual Foresight.

Black-box attacks. Black-box adversaries do not have access to π_v ’s network parameters or architecture. Multiple black-box attack methods based on finite-difference method were proposed in [26]. These methods require both reverting the environment to a previous state and making unlimited queries to π_v , which is not possible in real-time. Other black-box methods [10, 29] use proxy models to approximate π_v . Adversarial perturbations are generated from these proxy models. These two attack methods still have the same issue of having to compute a perturbation for every state, making it slower than v ’s response time.

7. Conclusion

We showed that our proposed techniques, UAP-S and UAP-O, which use universal perturbations, are effective in fooling DRL policies in real-time. Unlike state-of-the-art attacks, our techniques are based on a realistic adversary model. We also demonstrated current defense mechanisms are not effective against attacks based on universal perturbations. The attacks discussed in this paper assume that the adversary has white-box access to the victim DRL policy. We plan to extend our attacks to the black-box case and continuous control by first mounting a model extraction attack and then applying our current techniques to find transferable universal perturbations. The insights we presented in Section 2.4, can be used as the basis to build a comprehensive defense that can both detect and mitigate universal perturbation-based adversarial example attacks against DRL agents.

References

- [1] Shumeet Baluja and Ian Fischer. Learning to attack: Adversarial transformation networks. In *AAAI*, pages 2687–2695, 2018.
- [2] Vahid Behzadan and Arslan Munir. Vulnerability of deep reinforcement learning to policy induction attacks. In *International Conference on Machine Learning and Data Mining in Pattern Recognition*, pages 262–275. Springer, 2017.
- [3] Vahid Behzadan and Arslan Munir. Whatever does not kill deep reinforcement learning, makes it stronger. *arXiv preprint arXiv:1712.09344*, 2017.
- [4] Marc G Bellemare, Yavar Naddaf, Joel Veness, and Michael Bowling. The arcade learning environment: An evaluation platform for general agents. *Journal of Artificial Intelligence Research*, 47:253–279, 2013.
- [5] Nicholas Carlini and David Wagner. Towards evaluating the robustness of neural networks. In *2017 IEEE Symposium on Security and Privacy (SP)*, pages 39–57. IEEE, 2017.
- [6] Prafulla Dhariwal, Christopher Hesse, Oleg Klimov, Alex Nichol, Matthias Plappert, Alec Radford, John Schulman, Szymon Sidor, Yuhuai Wu, and Peter Zhokhov. Openai baselines. <https://github.com/openai/baselines>, 2017.
- [7] Ian Goodfellow, Jonathon Shlens, and Christian Szegedy. Explaining and harnessing adversarial examples. In *International Conference on Learning Representations*, 2015.
- [8] Sandy Huang, Nicolas Papernot, Ian Goodfellow, Yan Duan, and Pieter Abbeel. Adversarial attacks on neural network policies. *arXiv preprint arXiv:1702.02284*, 2017.
- [9] Leonard Hussenot, Matthieu Geist, and Olivier Pietquin. Copycat: Taking control of neural policies with constant attacks. In *International Conference on Autonomous Agents and Multi-Agent Systems (AAMAS)*, 2020.
- [10] Matthew Inkawhich, Yiran Chen, and Hai Li. Snooping attacks on deep reinforcement learning. *arXiv preprint arXiv:1905.11832*, 2019.
- [11] Jernej Kos and Dawn Song. Delving into adversarial attacks on deep policies. *arXiv preprint arXiv:1705.06452*, 2017.
- [12] Solomon Kullback and Richard A Leibler. On information and sufficiency. *The annals of mathematical statistics*, 22(1):79–86, 1951.
- [13] Yen-Chen Lin, Zhang-Wei Hong, Yuan-Hong Liao, Meng-Li Shih, Ming-Yu Liu, and Min Sun. Tactics of adversarial attack on deep reinforcement learning agents. *arXiv preprint arXiv:1703.06748*, 2017.
- [14] Yen-Chen Lin, Ming-Yu Liu, Min Sun, and Jia-Bin Huang. Detecting adversarial attacks on neural network policies with visual foresight. *arXiv preprint arXiv:1710.00814*, 2017.
- [15] Volodymyr Mnih, Adria Puigdomenech Badia, Mehdi Mirza, Alex Graves, Timothy Lillicrap, Tim Harley, David Silver, and Koray Kavukcuoglu. Asynchronous methods for deep reinforcement learning. In *International conference on machine learning*, pages 1928–1937, 2016.
- [16] Volodymyr Mnih, Koray Kavukcuoglu, David Silver, Andrei A Rusu, Joel Veness, Marc G Bellemare, Alex Graves, Martin Riedmiller, Andreas K Fidjeland, Georg Ostrovski, et al. Human-level control through deep reinforcement learning. *Nature*, 518(7540):529, 2015.
- [17] Seyed-Mohsen Moosavi-Dezfooli, Alhussein Fawzi, Omar Fawzi, and Pascal Frossard. Universal adversarial perturbations. In *Proceedings of the IEEE conference on computer vision and pattern recognition*, pages 1765–1773, 2017.
- [18] Seyed-Mohsen Moosavi-Dezfooli, Alhussein Fawzi, and Pascal Frossard. Deepfool: a simple and accurate method to fool deep neural networks. In *Proceedings of the IEEE conference on computer vision and pattern recognition*, pages 2574–2582, 2016.
- [19] Nicolas Papernot, Patrick McDaniel, Somesh Jha, Matt Fredrikson, Z Berkay Celik, and Ananthram Swami. The limitations of deep learning in adversarial settings. In *2016 IEEE European symposium on security and privacy (EuroS&P)*, pages 372–387. IEEE, 2016.
- [20] Olga Russakovsky, Jia Deng, Hao Su, Jonathan Krause, Sanjeev Satheesh, Sean Ma, Zhiheng Huang, Andrej Karpathy, Aditya Khosla, Michael Bernstein, et al. Imagenet large scale visual recognition challenge. *International journal of computer vision*, 115(3):211–252, 2015.
- [21] John Schulman, Filip Wolski, Prafulla Dhariwal, Alec Radford, and Oleg Klimov. Proximal policy optimization algorithms. *arXiv preprint arXiv:1707.06347*, 2017.
- [22] Jianwen Sun, Tianwei Zhang, Xiaofei Xie, Lei Ma, Yan Zheng, Kangjie Chen, and Yang Liu. Stealthy and efficient adversarial attacks against deep reinforcement learning. *arXiv preprint arXiv:2005.07099*, 2020.
- [23] Richard S. Sutton and Andrew G. Barto. *Reinforcement Learning: An Introduction*. The MIT Press, second edition, 2018.
- [24] Christian Szegedy, Wojciech Zaremba, Ilya Sutskever, Joan Bruna, Dumitru Erhan, Ian Goodfellow, and Rob Fergus. Intriguing properties of neural networks. In *International Conference on Learning Representations*, 2014.
- [25] Edgar Tretschk, Seong Joon Oh, and Mario Fritz. Sequential attacks on agents for long-term adversarial goals. *arXiv preprint arXiv:1805.12487*, 2018.
- [26] Chaowei Xiao, Xinlei Pan, Warren He, Jian Peng, Mingjie Sun, Jinfeng Yi, Bo Li, and Dawn Song. Characterizing attacks on deep reinforcement learning. *arXiv preprint arXiv:1907.09470*, 2019.
- [27] Huan Zhang, Hongge Chen, Chaowei Xiao, Bo Li, Mingyan Liu, Duane Boning, and Cho-Jui Hsieh. Robust deep reinforcement learning against adversarial perturbations on state observations. In *Advances in Neural Information Processing Systems*, volume 33, pages 21024–21037. Curran Associates, Inc., 2020.
- [28] Xiangyu Zhang, Jianhua Zou, Kaiming He, and Jian Sun. Accelerating very deep convolutional networks for classification and detection. *IEEE transactions on pattern analysis and machine intelligence*, 38(10):1943–1955, 2015.
- [29] Yiren Zhao, Ilia Shumailov, Han Cui, Xitong Gao, Robert Mullins, and Ross Anderson. Blackbox attacks on reinforcement learning agents using approximated temporal information. In *2020 50th Annual IEEE/IFIP International Conference on Dependable Systems and Networks Workshops (DSN-W)*, pages 16–24. IEEE, 2020.

Appendix

A. Proof of Equation 6

In this section, we provide a formal proof of Equation 6 that was used to find the perturbation in UAP-O.

In UAP-O, we defined an additional constraint for the perturbation as $\tilde{r}_j = \tilde{r}_k$, $\forall j, k \in \{t-N+1, \dots, t\}$, so that the same \tilde{r}_j is applied into all observations o_j . As pointed out in Section 3.2, at i -th iteration, the DeepFool algorithm computes the i -th perturbation \mathbf{r}_i for i -th state \mathbf{s}_i as

$$\mathbf{r}_i \leftarrow \frac{|\pi'_i|}{\|\mathbf{w}'_i\|_2^2} \mathbf{w}'_i. \quad (7)$$

UAP-O finds the closest $\tilde{\mathbf{r}}_i$ to \mathbf{r}_i by minimizing both $\|\mathbf{w}'_i\|_2^2 - \|\tilde{\mathbf{r}}_i\|_2^2$ and $\|\mathbf{w}'_i - \tilde{\mathbf{r}}_i\|_2^2$ in order to approximate the magnitude $|\pi'_i|/\|\mathbf{w}'_i\|_2^2$ and the direction \mathbf{w}'_i of \mathbf{r}_i . We can remove the square term and equivalently minimize only l_2 norms. Using the reverse triangular inequality in

$$\|\mathbf{w}'_i\|_2 - \|\tilde{\mathbf{r}}_i\|_2 \leq \|\mathbf{w}'_i - \tilde{\mathbf{r}}_i\|_2, \quad (8)$$

it is sufficient to solve $\min \|\mathbf{w}'_i - \tilde{\mathbf{r}}_i\|_2$ to find an optimal $\tilde{\mathbf{r}}_i$.

We can find the optimal $\tilde{\mathbf{r}}_i$ by setting partial derivatives $\partial \|\mathbf{w}'_i - \tilde{\mathbf{r}}_i\|_2 / \partial \tilde{r}_{i_j}$ to zero for all $j \in \{t-N+1, \dots, t\}$, where N denotes the total number of observations inside state \mathbf{s} . We also set all \tilde{r}_{i_j} into the same variable \tilde{r}_{i_t} . Therefore, we simply obtain $\tilde{\mathbf{r}}_{i_t}$ by finding the point where the partial derivative is equal to zero.

$$\begin{aligned} \frac{\partial \|\mathbf{w}'_i - \tilde{\mathbf{r}}_{i_t}\|_2}{\partial \tilde{r}_{i_t}} &= \frac{\partial ((\mathbf{w}'_{i_t} - \tilde{\mathbf{r}}_{i_t})^2 + \dots + (\mathbf{w}'_{i_{t-N}} - \tilde{\mathbf{r}}_{i_t})^2)^{1/2}}{\partial \tilde{r}_{i_t}} \\ 0 &= \frac{\partial f(\tilde{r}_{i_t})^{1/2}}{\partial \tilde{r}_{i_t}} \\ 0 &= 0.5f(\tilde{r}_{i_t})^{-3/2}(2(N+1)\tilde{r}_{i_t} - 2 \sum_{k=t-N+1}^t \mathbf{w}'_{i_k}) \end{aligned} \quad (9)$$

The squared difference function $f(\tilde{r}_{i_t})^{-3/2} \geq 0$ and only equal to zero when $\tilde{r}_{i_t} = \mathbf{w}'_{i_k}$ for all k . Even if $\mathbf{w}'_{i_k} = \tilde{\mathbf{r}}_{i_t}$, $\forall k \in \{t-N+1, \dots, t\}$, UAP-O computes the perturbation at i -th iteration as

$$\tilde{\mathbf{r}}_{i_t} = 1/N \sum_{k=t-N+1}^t \mathbf{w}'_{i_k}. \quad (10)$$

B. Experimental Setup

To facilitate the comparative performance of different attacks presented in Section 4, we used PyTorch (version

1.2.0) [39], NumPy (version 1.18.1) and Gym (a toolkit for developing reinforcement learning algorithms, version 0.15.7) libraries. All experiments are done in a computer with 2x12 core Intel(R) Xeon(R) CPUs (32GB RAM) and NVIDIA Quadro P5000 with 16GB memory.